Transmit Coil Decoupling of 8-Channel Coil Arrays with Ultra-Low Output Impedance RF Power Amplifiers

D. Yeo[1], E. Fiveland[1], R. Giaquinto[1], T. Song[2], X. Yang[2], K. Park[1], A. B. Kerr[3], X. Chu[2], and I. Hancu[1]
[1]GE Global Research, Niskayuna, NY, United States, [2]GE Global Research, Shanghai, China, People's Republic of, [3]Department of Electrical Engineering, Stanford University, Stanford, California, United States

Introduction: In previous work, an ultra-low output impedance RF power amplifier (RFPA) was introduced to reduce the effects of inter-element inductive coupling in parallel transmit arrays [1]. It uses an output-matching network to transform the MOSFET drain-source impedance into a very low value to suppress inter-element coupling effects while matching the coil input impedance to the optimum load of the MOSFET to maximize the available output power. In this work, we compare the decoupling improvement between the ultra-low output impedance (ULOI) RFPAs and conventional RFPAs under different loading conditions. Bench tests and imaging studies were performed on a 3T MR scanner (GE MR750, GE Healthcare, Waukesha, WI, USA) with 8-channel transmit and receive flat array and cylindrical coils. A B_1^+ image-based decoupling measure was computed for all the imaging experiments, and compared to the scattering parameters (S_{21}) between coil elements.

Methods: Two sets of 8-channel transmit/ receive flat array and cylindrical coils (Fig. 1) were tuned (127.74MHz) and matched to work with the ULOI RFPAs or conventional RFPAs, respectively. In the first set of experiments, the coils were driven by 8 conventional RFPAs via circulators, presenting 50Ω impedances to the coil ports. In the second set of experiments, the coil elements were driven directly by 8 ULOI RFPAs. Each flat array coil had two underlapped columns (center gap=19mm) of 4 overlapped loop coils (90mm x 93mm, trace width = 5mm) and was placed on a rectangular block phantom (510mm×405mm×170mm) filled with DI water, 1gm/L $CuSO_4$, and, NaCl. For each RFPA type, the NaCl concentration was adjusted to obtain coil loading values of 35Ω, 50 Ω, and, 65Ω. The cylindrical array (dia=28cm) consisted of 8 overlapped loop coils (length =308mm, width=134.4mm, trace width=5mm). Six experiments were performed for each coil array type (2 RFPA types×3 load values). In each experiment, each coil array's S_{21} parameters were measured, and, 8 B_1^+ maps of individually excited coil elements were acquired on the scanner.

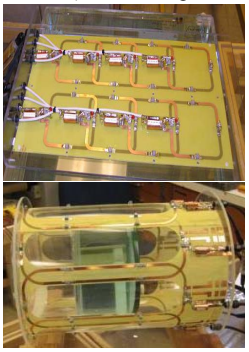

Fig. 1. Eight-channel (top) flat array and (bottom) cylindrical coils.

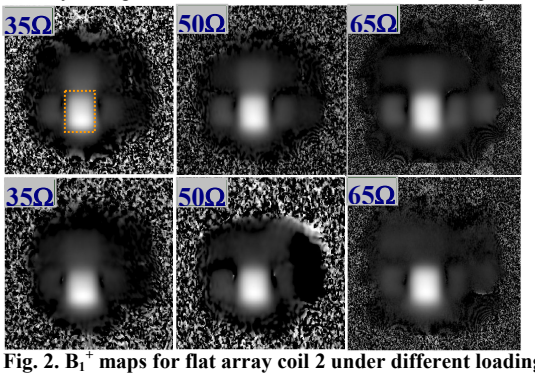

Fig. 2. B_1^+ maps for flat array coil 2 under different loading conditions for (top) conventional and (bottom) low output impedance RFPAs. Identical display scales are used.

Table 1. B_1^+-based coupling matrix for flat array

Tx coil	Rx1	Rx2	Rx3	Rx4	Rx5	Rx6	Rx7	Rx8
1	**1.00**	0.08	0.05	0.01	0.25	0.10	0.03	0.01
2	0.17	**1.00**	0.15	0.03	0.09	0.23	0.06	0.03
3	0.01	0.15	**1.00**	0.18	0.01	0.07	0.25	0.16
4	0.01	0.06	0.14	**1.00**	0.01	0.01	0.09	0.27
5	0.07	0.08	0.01	0.01	**1.00**	0.16	0.04	0.02
6	0.01	0.00	0.05	0.01	0.21	**1.00**	0.18	0.01
7	0.01	0.01	0.14	0.01	0.06	0.20	**1.00**	0.20
8	0.01	0.01	0.01	0.18	0.01	0.05	0.22	**1.00**

Table 2. Decoupling improvement for 8-channel flat array coils using B_1^+-based coupling matrix for different loads and RFPAs.

	Mean of Sum of Rows in Coupling Matrix		Decoupling Improvement (%)
Load	Conventional RFPA	Low Z_{out} RFPA	
35 Ω	0.125	0.085	32.0
50 Ω	0.127	0.102	19.7
65 Ω	0.179	0.136	24.0

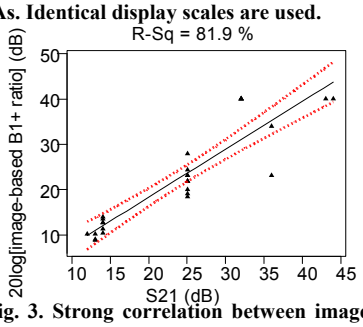

Fig. 3. Strong correlation between imaged based coupling and S_{21} values (dotted lines - 95% CI) for conventional RFPA with 35Ω load for flat array.

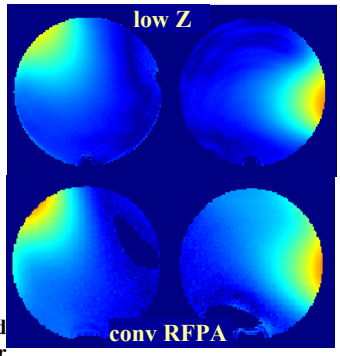

Fig. 4. B_1^+ maps for two individually excited (left, right) channels in cylindrical coil driven by (top) ultra-low output impedance and (bottom) conventional RFPAs. Same display scale used for all images.

Results and Discussion: In the imaging experiments, inter-element coupling in the flat array was measured by applying a normalization constant to a rectangular region of the B_1^+ map over the transmitting coil (Fig. 2) such that the mean image intensity in the region was 1.0. By sliding the window over each of the remaining coils and computing the mean intensities after applying the same normalization constant within the window, an imaged-based coupling matrix was created (Table 1). It contains the fractional values of the mean normalized B_1^+ value under each non-transmitting element with respect to each transmitting element – analogous to an S_{21} table. Brighter B_1^+ regions under non-transmitting coils will yield higher values in the table. The mean of the sum of all the rows in these tables were evaluated to assess the decoupling improvement for the six experiments (Table 2). The mean image-based coupling per transmitting element (left, middle columns in Table 2) and S_{21} tables indicated that inter-element coupling increased with increasing loads for both RFPAs. However, for each loading condition, the conventional RFPAs yielded poorer transmit decoupling performance (higher values in Table 2). The ULOI RFPAs yielded between 19.7% to 32.0% B_1^+ decoupling improvement over conventional RFPAs in the flat array coils (right column in Table 2). When converted to decibels, the values in the six imaged-based coupling tables were strongly correlated to the S_{21} tables (Fig. 3), which presents the potential to use these two methods as complimentary means to relate bench results to transmit fields observed in the scanner. Linear regression of identically located cells in both sets of six tables yielded a mean R^2 value of 0.72 (max=0.84, min=0.46, p=0.0001). This is reasonable since the coupling-induced B_1^+ values were proportional to the induced coil currents, which were related to the coil port voltages from which the S_{21} values were derived. Fig. 4 shows B_1^+ maps of a cylindrical phantom in the cylindrical coil when two elements were individually excited. Relative to the ULOI RFPAs, the conventional RFPAs yielded B_1^+ distributions with brighter regions under non-transmitting coils due to stronger coupling-induced currents. We are currently studying the benefits of the improved transmit decoupling in key parallel transmit applications. The ULOI RFPAs exhibit stronger current source behavior [1] when the impedance seen by the coil port is higher, i.e., impedance seen by the coil's matching network, looking towards the RFPA, is lower. Shortening the cables from the RFPA to the coil may reduce the latter impedance and provide stronger decoupling performance. This can be achieved with non-magnetic RFPAs placed in the magnet room.

Conclusions: Using B_1^+ imaging measurements, the ULOI RFPAs were found to provide up to 32% improvement in inter-element transmit decoupling in our experimental setup. The logarithms of the B_1^+-based coupling matrices were found to be strongly correlated to the S_{21} parameters measured on the bench.

References: [1] Chu X, et. al., IEEE TMI, 2009. **Acknowledgement:** This work was funded by NIH grant R01EB005037.